Quantifying water cover shifts across the globe: following the steps of walking floods

P. Torre Zaffaroni[1,2,3], J. Houspanossian[3], C.M. Di Bella[1,2], E.G. Jobbágy[3]

[1]Instituto de Investigaciones Fisiológicas y Ecológicas Vinculadas a la Agricultura (IFEVA), Facultad de Agronomía, Universidad de Buenos Aires, CONICET, Buenos Aires, Argentina
[2]Departamento de Métodos Cuantitativos y Sistemas de Información, Facultad de Agronomía, Universidad de Buenos Aires
[3]Grupo de Estudios Ambientales – IMASL, Universidad Nacional de San Luis & CONICET, San Luis, Argentina

Key Points:

- We developed two complementary indices to describe water cover shifts between and within flooding events
- Over the last 36 years, shifts expanded the global flooded-affected area by 25% with another 20% redistributing at intermediate stages
- Flat topographies, arid climates, and irrigation favor this phenomenon while river dams and channels inhibit it over time

Corresponding author: Paula Torre Zaffaroni, torrezaffaroni@agro.uba.ar

Abstract

Floods in ideal landscapes follow a coherent pattern where single water-covered areas expand and afterwards recede following the inverse sequence but deviate in real landscapes, due to natural or human factors, resulting in flood coverage shifts. Using remote sensing, we introduced two indices to describe the discrepancies between spatially integrated vs. pixel-level frequency distributions under maximum flooded conditions (dext) and throughout all flooding conditions (dtot), expressed as the relative weight of shifts on each landscape's maximum registered coverage, theoretically ranging between no displacement (<20%) to maximum displacement (<< inf). Globally, over 36 years floods exhibited redistributions representing, on average, 25% and 45% of their peak extents revealing previously unnoticed extra flooded areas and rotational movements within flooding events, rising up to 500% in meandering rivers (South America) and irrigated croplands (Central Asia). We also assessed the influence of natural and human variables and discussed the indices' potential for advancing flood research.

Plain Language Summary

While in ideal landscapes flood events should display the same spatial distribution in their expansion and recession stages of any flooding event, real flooding may drift away from this expected pattern. We developed two indices based on remote sensing data to locate where these shifts are important and understand how they are influenced by nature and humans. By analyzing data from around the world, we discovered that thanks to the displacement from the ideal distributions, floods covered globally an extra quarter of the area. Natural factors like low terrain ruggedness and high aridity foster much larger flooding displacement. In regions hosting rivers that carry large quantities of sediment and often change their course (e.g., India and Perú), displacement engages five times more area in floods than ideally expected. We also found that water infrastructure like reservoirs and irrigation also influenced flooding displacement. For instance, displacement was very relevant in intensely irrigated regions like Central Asia and Australia, reflecting surface water deviation as needed for crop production. Because these variations scope flooding spatiotemporal dynamics with important implications for the provision of many ecosystem services, their quantification and assessment allow us to monitor and understand our ongoing imprint on regional flooding dynamics.

1 Introduction

The spatial dynamics of floods, and specifically the pattern of their expansion and recession over the territory, is an important aspect of flooding variability. The flood pulse concept describes a model of flooding where water increasingly covers adjacent areas of already flooded surfaces, and afterward recedes following the exact inverse sequence, along what is described as an aquatic-terrestrial transition zone (Junk et al., 1989; Wantzen et al., 2008, for a definition extended to lentic systems). This null model of fully coherent flood expansion/recession implies that the exact locations that are covered by water can be known for any level of flooding (i.e., any given fraction of water coverage) based on the distribution of previous floods. However, in real landscapes like those occupied by highly meandering rivers, floods do not always proceed in this predictable way, changing locations throughout successive events or by following asymmetrical expansion vs. recession trajectories (Tockner et al., 2000; Finotello et al., 2020). Though it could give important insights into ecosystem functioning at multiple levels, this attribute of flooding dynamics (hereafter, flooding displacement) has not yet been systematically quantified, and has been seldom described in the case of shallow lakes. Instead, flooding displacement has been analyzed in riverbanks through numerical modeling (Camporeale et al., 2005), manual and automatized detection of spatial shifts of water-classified pixels (Lin et al., 2020; Langhorst & Pavelsky, 2023), or, more commonly, included as a known

attribute in the design of field experiments and observations (Constantine & Dunne, 2008; Finotello et al., 2020; Walcker et al., 2021) from which a large body of knowledge on the physical laws guiding displacement has been generated (Wren et al., 2008; Van Dijk et al., 2013).

The spatiotemporal nature of this phenomenon suggests that it can be explored through remote sensing. A key advantage is its ability to uniformly study one attribute with low costs. With the development of global water masks from the Landsat satellite archive (Pekel et al., 2016a) and cloud processing servers (Gorelick et al., 2017), it is possible to analyze flooding displacement globally for more than three decades. Such information has already helped to explore the temporal dynamics of floods, including long-term trends (Pekel et al., 2016a; Olthof & Rainville, 2022) and other components of temporal variability (Pickens et al., 2020, Torre Zaffaroni et al., in review, submitted to Water Resources Research, 2023), and even colorimetric characterizations as a proxy of water quality (Gardner et al., 2021). Moreover, Langhorst and Pavelsky (2023) have shown that the displacement of riverbeds can be assessed through remote sensing, quantifying the direction of erosion and accretion for water courses wider than 100m with excellent results. These studies showcase how optical remote sensing tools can detect detailed aspects of flooding, presenting an opportunity for comprehensive global characterizations and studies of geographical drivers, despite their limitations such as data gaps caused by cloud coverage and lower resolution for older satellite missions.

While climate, topography, and water infrastructure have been pointed out as drivers of flooding displacement, their relative importance in dictating how floods drift away from a coherent regime remains unquantified. In the case of dry regions high runoff and precipitation variability translate into spatially heterogeneous flood events (Tooth, 2000; Brunsell, 2010). Rivers in plains with high geomorphological activity can carry, remove, and deposit large amounts of sediment in their banks fostering migration of courses and the formation of oxbow lakes which retain large masses of water (Richardson et al., 1987; Constantine & Dunne, 2008; Langhorst & Pavelsky, 2023). Because slope, ruggedness, and landforms at a landscape level dictate surface water transport and storage (McGuire et al., 2005; Sivapalan et al., 2011; Rudorff et al., 2014), we hypothesize that topographic characteristics are important determinants of flooding displacement beyond lotic systems. On top of natural drivers, irrigation, particularly in paddy rice cultivation, can contribute to flooding displacement due to varying watering practices in different plots, especially in regions that practice double and triple cropping systems (Sakamoto et al., 2007; Dong et al., 2015). River engineering, such as channelization, canalization, dams, and reservoirs can minimize flooding displacement by altering river geomorphology and sediment transport downstream (Ward & Stanford, 1995; Vörösmarty et al., 2010; Tena et al., 2020).

As flood expansion/recession cycles sustain many ecosystemic functions (Tockner & Stanford, 2002; Pi et al., 2022) including the exchange of greenhouse gases with the atmosphere (Watts et al., 2014; Saunois et al., 2020; Walcker et al., 2021), it is important to quantify how floods displace over time to better forecast changes in ecosystem function as well as global climate. Remote sensing tools make it feasible to monitor the response of flooding to increasingly variable precipitation regimes (Kundzewicz, 2008; Najibi & Devineni, 2018; Arias et al., 2021), changes in land use and land cover (Twine et al., 2004; Loarie et al., 2011; Kuppel et al., 2015), and mitigation-oriented water management strategies. It can further improve decision-making for flood management and planning by improving the identification of flood-prone areas and their shift across landscapes.

This work addresses the spatial dynamics of floods focusing on flooding displacement across events. First, it builds two indices that quantify the degree to which the distribution of floods deviates from a fully coherent expansion/recession pattern (i.e., flooding displacement). Second, it maps flood displacement with these indices over the last 36 years for the whole globe using remotely sensed data of surface water and evaluates

their conjoint performance across gradients of coherence. Finally, it explores how flooding displacement relates to natural and anthropic factors. The ultimate goal is to set the methodological basis for studying flood displacement patterns and trends using long-term data of global scope.

2 Data and Methods

We based our work on high-resolution, remotely sensed data of surface water coverage, using spatially aggregated (single pixels within a grid cell) time series vs. temporally aggregated (single dates across the whole study period) pixel distributions to quantify displacement. The monthly, 30-meter resolution Global Surface Water Extent dataset (Pekel et al., 2016a) is a powerful tool to analyze regional-level flooding processes, with available observations going back as far as 1985. Its most recent version (v1.4) extended the original version up to 2021, inclusive, and can be found in the Google Earth Engine catalog, the latter which allows the processing of such vast amounts of data.

A spatially coherent development of floods should reflect a bucket-like geometry where, as the flooded area increases, places that were already flooded stay covered by water, and where one can observe the same distribution of water-covered and water-free areas for any given fraction of total water coverage in the region in all flood episodes and regardless of being in the expansion or retraction phase (Figure 1b). In such cases, when flooded areas are aggregated for a given extent of the territory (e.g., catchment or grid cell) the overall floodable area (sum of all the individual pixels that were covered by water at any point in the time period) should match the maximum flooded extent (sum of all the pixels that were covered by water when flooding reached its maximum coverage in the region), and the recession of flooding should mirror its development exactly with the first drying areas being the last ones that got flooded. Taking this hypothetical situation as a null model, we measured two aspects through which departures from this pattern can emerge. The accompanying schematization for three alternative hypothetical situations is found in Figure 1 (c-e). First, we defined the extreme displacement (d_{ext}) as the relative difference between the overall flooded extent (O), which is the sum of all pixels that were covered by water at any point in time, and the maximum extent observed simultaneously at any particular month in the spatially-aggregated time series (Mx) (Eq. 1).

$$d_{ext} = \frac{O - Mx}{Mx} \tag{1}$$

This index represents the fraction of area that escaped some individual peak events but was still engaged in flooding and is assumed to have been gained from the dry fraction of the landscape. It is easily interpreted as the fraction of the area that missed the flood at the time of maximum coverage, providing valuable information about the wetting-drying dynamic of the region. For this reason, it should be more sensitive for analyzing individual events or dynamics in which different fractions of the landscape engage in each flood event, more commonly found in irrigated landscapes (Figure 1c).

The previous extreme displacement quantification may underestimate flood displacement taking place at intermediate levels of water coverage or highly rotating floods, such as those experienced in high-intensity irrigated landscapes where the flooding sequence of plots is erratic (Figure 1d). It could also fall short of capturing flood dynamics where engaged areas may converge beyond a certain threshold of water coverage but not below it (i.e., yielding $d_{ext} = 0$; Figure 1e), and where still the observed apportionment of flooding frequency among pixels differs greatly from a coherent pattern. In such cases, the exceeding area does not result just from the dry fraction of the landscape but also from what we would expect to be highly flooded areas, producing more temporary wa-

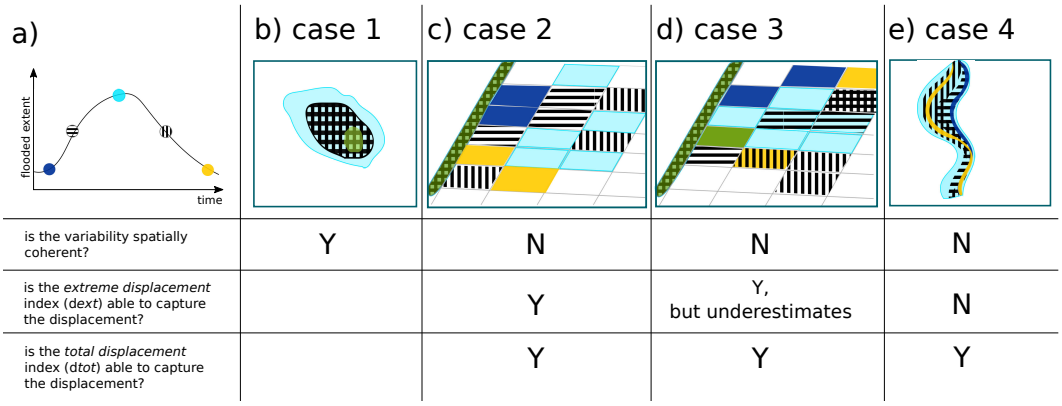

Figure 1. Four alternative hypothetical configurations of flooding for the same temporal series of spatially-aggregated water coverage (a). Cases include: (b) coherent flooding dynamic where the last flooded areas are the first to dry, commonly observed in lakes; (c) incoherent flooding dynamic where each plot is flooded in a rotative way such that each one is covered by water at only one time-step, a situation that could take place in low-to-medium intensity irrigated regions; (d) incoherent flooding dynamic where plots are alternately and variably flooded, a situation expected in high intensity irrigated regions; (e) incoherent flooding dynamic where the spatial pattern of the wetting and drying phase diverges, which can be expected in branched and meandering rivers and their surrounding floodplains as well as hydrologically connected wetlands. Coherence and the ability of the two indices (d_{ext} and d_{tot}) to capture displacement are indicated (yes/no).

ter bodies than expected by the information extracted from a spatially aggregated flood time series.

Given the potential underestimation of displacements by the first index presented above, we constructed a total displacement index (d_{tot}) by comparing two different flooded area frequency distributions. The first one (temporal distribution, T) results from rearranging the time series of monthly surface water extent in a decreasing array. Assuming a null model where the aggregated monthly flood extent accurately represents the flooding dynamics within the region, this rearrangement would show (1) the maximum floodable area (i.e., the first observation where all pixels that can be flooded are flooded); (2) the minimum flooded area or permanent water fraction (i.e., the lowest extent observed, which could also be zero); and (3) the flooding frequency distribution per fraction of area, which is obtained by calculating the difference between observations, starting from the maximum. For example, a region where the maximum observed event across 10 years (i.e., 120 monthly observations) accounted for 1% of the area and the next biggest event accounted for 0.9% of the area should show 0.1% of its area with a flooding frequency of 1/120 (0.83%). Then, if the null model is representative of the flooding dynamics in this region, T reflects the relative contribution of pixels with different individual flooding frequencies, which can be estimated independently by measuring the distribution of the actual flooding frequencies, as the percentage of observations with water, at the pixel level (30x30 m^2) (S). The mismatch between T and S can be quantified as shown in Eq. 2:

$$d_{tot} = \frac{\sum_0^{100} T_n - S_n}{Mx} \qquad for T_n > S_n$$

(2)

where T_n and S_n are the nth frequency flooded area according to the temporal and spatial distributions, respectively. We standardize the mismatches to the maximum surface water extent event (Mx) of the region, and thus d_{tot} expresses the equivalent fraction of Mx that floods as a result of changing water-covered area locations within and between flooding events.

The described phenomenon can be characterized across multiple spatial scales of analyses, comparing upper-level behavior's concordance with their lower-level components' dynamic (e.g., pixels in remotely sensed data). For this global scope study, we chose a large landscape scale as our focal level, arranging a 1-degree grid (˜ 111x111km at the Equator). After excluding cells that included the ocean surface (12,500 resulting cells), we obtained the landscape-level surface water extent for each cell and month between 1985 and 2021, and further filtered (i) time series, keeping observations with over 70% of data available across the cell, and (ii) grid cells, keeping those with over 0.1% of maximum surface water extent and 30 observations, to reduce noise effects. As a result, we analyzed 10,047 cells over all continents except Antarctica. To illustrate how the displacement indices can be applied, we investigated the impact of natural and human factors on flooding location changes within and between events. Boosted regression trees were used to relate flooding displacement with topographical, climatological, hydrological, and agricultural variables (see Supporting Information for more details). The processing of the surface water extent dataset was done in Google Earth Engine, and posterior analyses were completed in an R environment (R Core Team, 2021).

3 Results and Discussion

3.1 Flooding displacement characterization

Based on remote sensing data, we developed a novel way to study how floods move across land revealing that their displacement, at varying degrees, is a widespread phenomenon, not only relevant in riverbanks but also important in shallow lakes and irrigated areas worldwide. Both displacement indices developed (d_{ext} and d_{tot}) were able to capture patterns where flooded areas change location throughout events. Through these novel indices, we discovered that close-to-fully coherent flooding patterns (i.e., no displacement) took place in lotic systems including floodplain sections across the Kunene, Ob and Paraguay Rivers in Angola, Russia, and Paraguay, respectively (d_{ext} and d_{tot} < 0.2), while in other regions displacement was so large that it exposed to flooding up to five times more area than expected from a coherent pattern such as in the floodplains of the Ucayali and Purús rivers in South America (d_{ext} and $d_{tot} > 1$) known for their high sediment load and dynamic geomorphology. In lotic systems, flooding displacement could result from different expansion patterns associated with the alternance of water source (Tockner et al., 2000), or from hysteretic patterns (i.e. non-symmetrical expansion/recession trajectories) related with riverine geomorphology (Poole, 2010). Yet, this pattern was also extended to lentic systems, for instance those in the northern Undulating Pampas in Argentina composed of very shallow lakes where there is a delicate, water table-mediated flood-generating mechanism (Kuppel et al., 2015). This suggested the usefulness of the indices for discriminating sites in which different flooding mechanisms may prevail (Van Dijk et al., 2013; Wu et al., 2023), and even for comparing their actual development overtime against the simulations of their expected behavior (Camporeale et al., 2005; Rudorff et al., 2014).

Different flooding regimes fostering displacement became evident after comparing the performance of both indices across 10,047, 1°-gridded landscapes (Figure 2). Low values of both d_{ext} and d_{tot} were indicative of coherent patterns where floods expanded and receded following the same geometrical path, such as that in well-defined lake basins (Figure 2a & b). Increases in either index could be attributed to redistribution of flooding between events or within individual events. For instance, greater differences in favor of d_{tot} (Figure 2d-f) suggested shifting patterns with a maximum event that covers all floodable pixels, as a result of intense rainfall, snowmelt, or upstream runoff pulses (as exemplified in Figure 1e). The overlap of maximum and overall extents was almost perfect, yet as much as 40% of the overall floodable extent alternated over time. In certain riverplains (e.g., in sections of the Ob' River, Figure 2d), this behavior had a marginal impact, accounting for less than 20% of water cover shifts. Elsewhere, higher d_{tot} values illustrated the evaporative dynamics of the Eyasi Lake and Aral Sea in Eastern Africa and Central Asia (Figure 2e-f). This type of displacement was more representative of the greatest water-covered landscapes (Figure 2 top-left panel, blue points). Finally, visual interpretation of cells with very high values of d_{ext} and d_{tot} suggested their sensitivity to both natural and human imprints on the distribution of flooded areas (Figure 2g-i).

Flooding displacement indices complement common flooding attributes, highlighting the contribution of this novel approach (Figure S2). Typical indicators of flooding variability include minimum, mean, and maximum extents, and coefficient of variation derived from spatially-aggregated flooded extent time series (e.g., Papa et al., 2008, 2010; Pickens et al., 2020). Our quantitative assessment of flooding redistribution appeared to complement flooding analysis (i.e., were poorly correlated) based upon the aggregation of higher resolution data, independently of their magnitude (i.e., for rarely flooded regions as well as for those hosting floods across the entire landscape), or how temporally variable they were (i.e., from very stable to highly erratic floods). This was suggestive of the value of the indices as, for instance, ephemeral and shallow water bodies fluctuating in size and volume, but also in location -as the indices capture- tend to be

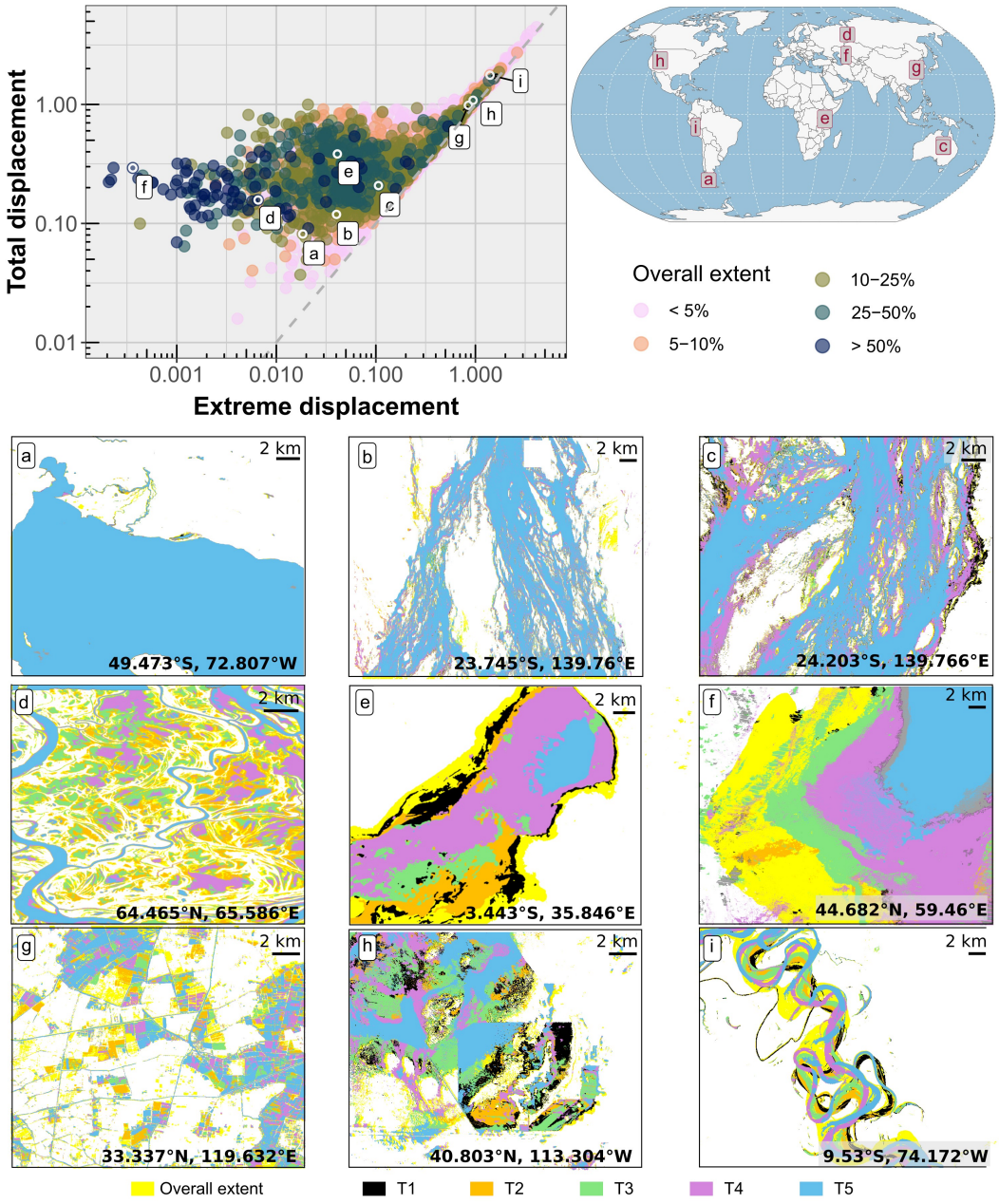

Figure 2. Values assumed for the two proposed flooding displacement indices (extreme displacement, d_{ext}, and total displacement, d_{tot}) across 10,047 1-degree landscapes. Top-right panel: log-log scatter plot coloring cells according to their overall flood extent (i.e., the fraction of area that has been flooded at least once in the last 36 years), with the gray dotted line reflecting the equality line between both indices. (a-i) Examples of the (mis)matches between the overall flooded extent (yellow background) and the geographical contribution of fractions of the landscape in five moments (T1 to T5). (a) Lake Viedma, Argentina; (b-c) Diamantina River, Australia; (d) Ob' River, Russia; (e) Eyasi Lake, Tanzania; (f) Aral Sea, Kazakhstan; (g) Zhenjiang, China (triple cropping hotspot); (h) Salt Flats, United States (partially exploited); (i) Ucayali River, Perú.

key contributors to greenhouse gas emissions (Saunois et al., 2020; Walcker et al., 2021), and whose wetting/drying dynamics may have been underestimated with current aggregation approaches (Davidson et al., 2018).

3.2 Global patterns of flooding displacement

Regional clusters of high flooding displacement became evident after mapping the two indices (d_{ext} and d_{tot}) globally (Figure 3). The general similarity between both indices suggested that the dominant displacement component is the shift of the water masses across events (e.g. Figure 1c), while erratic rotation (of river channels or irrigated plots, e.g., Figure 1d) has a secondary role and only in a subset of regions. The geographical distribution of flooding displacement showed river valleys in South America and Central Asia with the greatest degrees of displacement (captured by both indices, e.g., Figure 2g-i), followed by mountainous rivers and irrigation-dense regions further captured by the total displacement index (e.g., Figure 1d-e). The highest displacement took place in the tropics and subtropics including the Bermejo, Ganges, Orinoco, and Ucayali rivers in Argentina, India, Venezuela, and Peru, respectively. All these riverbeds host water courses that reach flat humid plains after leaving young mountain ranges with high sediment production (Chakrapani, 2005). Episodes of overflow in meandering and braided rivers that transport high contents of sediments periodically change their main and side courses, likely driving massive flood displacements in these areas (Constantine & Dunne, 2008).

Besides tropical and subtropical hotspots of displacement fostered by large, and geomorphologically dynamic riverplains, the rest of the world appeared less affected by shifts in the maximum water-covered area, as captured by d_{ext}, with an average of 0.25 (i.e., 25% more floodable area than that covered by their highest individual event). Yet, some regions were characterized by patterns in which displacement at intermediate flooding levels was more prominent (d_{tot} averaged 0.45) (Figure 2d-f). Examples of this behavior included the tundra shallow lakes region across the Canadian Shield and an irrigation-dense area along the northern edge of the Tibetan Plateau. Such cases were indicative of flooding patterns where, outside high pulses that covered all floodable areas, there may have been shifts overtime between flood pulses, for instance through the alternation of single, double, and triple rice cropping in rice-intensive regions (Sakamoto et al., 2007; Chen et al., 2012; Tran et al., 2018). The regional imprint of flood irrigation for cropland production was detected through flooded patches shifting along tropical rivers in Central Asia as well as in other displacement hotspots found in rivers of other parts of central Asia (Yarkand and Aksu), southeastern Australia (Murray), and eastern China (Yellow and Yangtze). These areas match some of the most infrastructure-dense landscapes as evidenced in literature and through visual interpretation of high-definition images (Siebert et al., 2015; Zeng et al., 2016; Liu, 2022).

Remarkably, the lowest displacement (d_{ext} and $d_{tot} < 0.3$) was characteristic of most of the boreal belt, especially across northern North America, Europe, and the vast majority of Russia. Local flooding dynamics were well captured at the landscape level with an approximate concentric expansion and retraction dynamic, possibly explained by the temperature-dominated (as opposed to precipitation-dominated) timing of floods (Papa et al., 2008; Kireeva et al., 2020, Torre Zaffaroni et al., in review, submitted to Water Resources Research, 2023) as well as the glacial processes that have shaped the topography of these landscapes in the past (i.e., a currently inactive geomorphological agent) that may constrain flooding to well-defined paths water follows (Buttle et al., 2016; Blöschl et al., 2020).

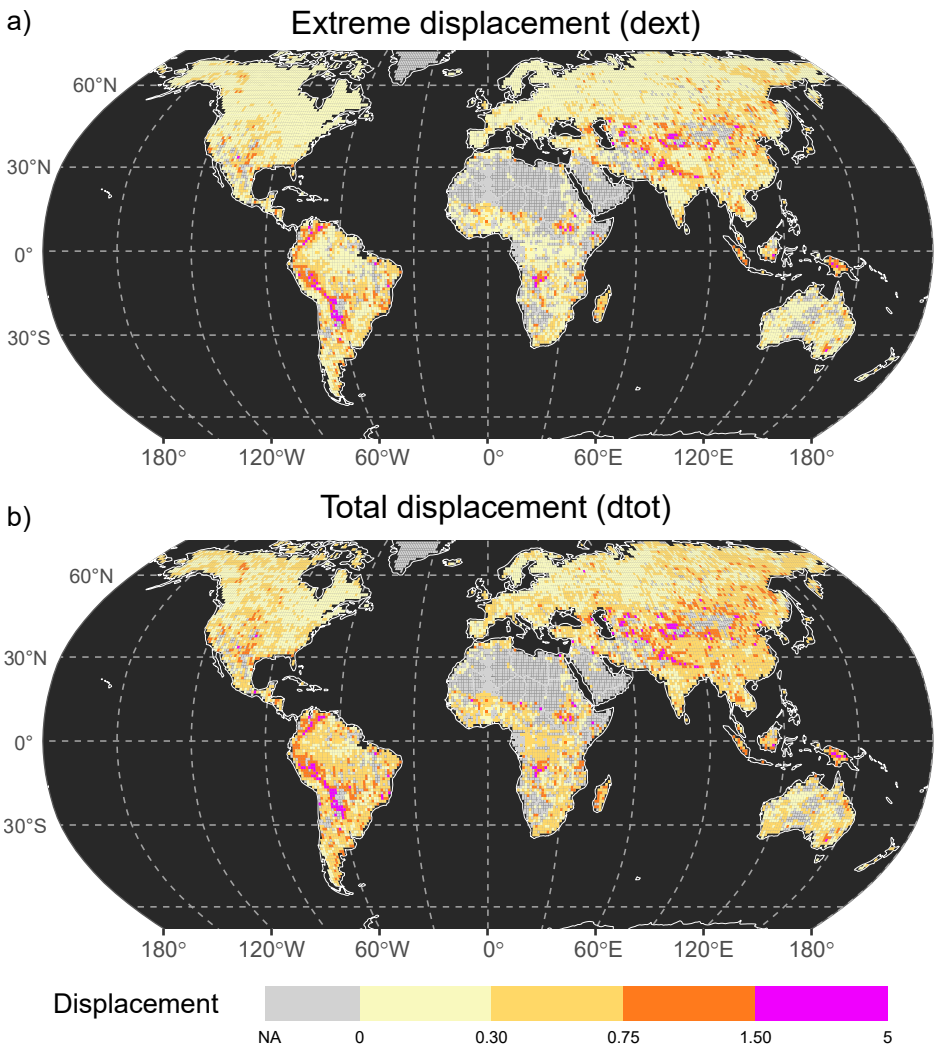

Figure 3. Global distribution of flooding displacement as described by two indices, (a) by obtaining the overall flooded area exceeding the maximum observed flooded area at any particular month (extreme displacement, d_{ext}), (b) by quantifying mismatches between the distribution of flooded frequency pixels and a null model given by the arrangement of landscape-aggregated time series of flooded extent (total displacement, d_{tot}). An interactive online map is available at `https://torrezaffaroni.users.earthengine.app/view/walking-floods`

3.3 Natural vs. human drivers of flooding displacement

Globally, natural drivers were on average more influential on flooding displacement than human drivers related to water management practices as shown by boosted regression trees (Figure S3, see Supplementary Information for more details). Across natural drivers, lake fraction, and local and regional indicators of ruggedness were the most important controls on flooding displacement. Extremely flat regions (regional terrain ruggedness index $<$ 80m), despite pronounced local slopes, foster flooding displacement, aligning with the slower convergence effect observed in the absence of well-defined drainage systems (Figure S4) (McGuire et al., 2005; Aragón et al., 2011). The average distance

between meanders, a quantitative indicator of river meandering, ranked fourth in influencing flooding displacement. This corroborated our observation that the indices can detect these highly dynamic landscapes, which provide numerous important ecosystem services worldwide (Opperman et al., 2010; Angelini et al., 2013; Walcker et al., 2021). Climate was strongly related to displacement, with aridity (mean annual precipitation to potential evapotranspiration ratio < 0.5) favoring it, perhaps as a result of the higher spatial variability of precipitation events causing floods (Tooth, 2000; Acworth et al., 2016; Griffin-Nolan et al., 2021).

Across human drivers, the density of reservoir and irrigation infrastructure diminished and enhanced flooding displacement, respectively, with the latter being more influential even than paddy for rice and rainfed agriculture (Figure S4). Irrigation management's impact on this aspect of flooding emphasizes the need to consider its role in regional hydrology modeling. This can enhance the representation of multiple land and atmospheric processes, including greenhouse gas emissions and local climate variability (Loarie et al., 2011; Houspanossian et al., 2018; Saunois et al., 2020). Our findings were similar for d_{ext} (Figure S5), with lake fraction exerting greater influence than river meandering, and floodplain and irrigation coverage, possibly due to the lower capacity of this index in capturing such displacement patterns (Figure 1d-e).

Furthermore, the proposed indices may help in exploring how displacement changes in a given landscape as it is modified either gradually (e.g., due to increasing irrigation-allocated areas) or more abruptly (e.g., due to dam emplacements). As an example, we explored the landscape encompassing two water infrastructure projects in central China (Three Gorges Dam, built on the Yangtze River between 1994 and 2003, and the Shuibuya Dam built on the Qingjiang River between 2002 and 2008), revealing a sharp decrease of flood displacement (d_{ext} from 1.42 to 0.43, Figure S6).

4 Conclusions

The distribution of floods within a landscape and its variation through time is a critical but neglected aspect of hydrological analysis and its significance can be overlooked when examining aggregated flooded areas over time. We tackled this gap by developing two indices, complementary to those typically employed to assess the temporal attributes of floods, that capture the disparities between the actual spatiotemporal distribution of flooded areas in a landscape and a null model of spatially coherent flooding in which water-covered areas expand and recede following symmetrical patterns in each event. Owing to this type of displacement, landscapes worldwide had 45% more area engaged in flooding episodes between 1985 and 2021 than what their single maximum flooding levels may have indicated. The highest additions occurred in South American and Asian landscapes dominated by large meandering rivers transporting sediments from some of the most tectonically active mountain ranges on Earth to their adjacent plains. Our results also showed that flat arid and tropical regions experienced the most significant displacement of flooded areas due to natural and human influences, while boreal regions had the most spatially coherent flooding events, likely due to their glacially-shaped landscapes.

Water coverage displacement characterization and its uniform application worldwide with the proposed indices have significant implications for understanding the influences of flooding on local and global climate as well as for evaluating the distant effects of land use change, such as deforestation and water infrastructure development, on hydrological regimes. Our indices demonstrate the potential applications through visual correspondence and explorative quantitative assessment. We hope to stimulate further research on this topic and contribute to a more comprehensive understanding of the complex dynamics of flooding in various landscapes. Our study underscores the need for more integral approaches to flood modeling and management.

5 Open Research

Global flooded extent was derived from JRC's Global Surface Water dataset v1.4 (Pekel et al., 2016b) available in the Google Earth Engine Data Catalog. Anthromes were downloaded from `https://dataverse.harvard.edu/dataset.xhtml?persistentId=doi:10.7910/DVN/GOQDNQ` (Ellis & Klein Goldewijk, 2019). River segment characterization was extracted from `https://zenodo.org/record/2582500` based on Global River Width from Landsat (Frasson et al., 2019). Global Lakes and Wetlands Database Level 3 (GLWD-3 Lehner & Döll, 2004) was downloaded from `https://www.worldwildlife.org/publications/global-lakes-and-wetlands-database-lakes-and-wetlands-grid-level-3` (Lehner & Döll, 2004). The aridity index was calculated based on TerraClimate long-term averages of annual precipitation-to-potential evapotranspiration ratios (Abatzoglou et al., 2018), while terrain attributes were calculated based on Global Multi-resolution Terrain Dataset (USGS), both available in the Google Earth Engine Data Catalog. The codes for characterizing displacement in Google Earth Engine and analyzing it in R, along with the database, with all variables aggregated to the 1-degree grid, can be found at `https://zenodo.org/record/8083689`.

Acknowledgments

This work was supported by CONICET (PIP 11220200100363CO, PIBBA 28720210100697CO). The authors declare no conflict of interest.

References

Abatzoglou, J. T., Dobrowski, S. Z., Parks, S. A., & Hegewisch, K. C. (2018). *Terraclimate: Monthly climate and climatic water balance for global terrestrial surfaces, university of idaho* [dataset]. Retrieved from `https://developers.google.com/earth-engine/datasets/catalog/IDAHO_EPSCOR_TERRACLIMATE` doi: 10.1038/sdata.2017.191

Acworth, R. I., Rau, G. C., Cuthbert, M. O., Jensen, E., & Leggett, K. (2016). Long-term spatio-temporal precipitation variability in arid-zone Australia and implications for groundwater recharge. *Hydrogeology Journal*, *24*(4), 905–921. doi: 10.1007/s10040-015-1358-7

Allen, G. H., & Pavelsky, T. (2018). Global extent of rivers and streams. *Science*, *361*(6402), 585–588. doi: 10.1126/science.aat063

Angelini, R., de Morais, R. J., Catella, A. C., Resende, E. K., & Libralato, S. (2013). Aquatic food webs of the oxbow lakes in the Pantanal: A new site for fisheries guaranteed by alternated control? *Ecological Modelling*, *253*, 82–96. doi: 10.1016/j.ecolmodel.2013.01.001

Aragón, R., Jobbágy, E. G., & Viglizzo, E. F. (2011). Surface and groundwater dynamics in the sedimentary plains of the Western Pampas (Argentina). *Ecohydrology*, *4*(3), 433–447. doi: 10.1002/eco.149

Arias, P., Bellouin, N., Coppola, E., Jones, R., Krinner, G., Marotzke, J., ... Zickfeld, K. (2021). *Technical summary* (Tech. Rep.). Geneva, Switzerland: The Intergovernmental Panel on Climate Change (IPCC).

Blöschl, G., Kiss, A., Viglione, A., Barriendos, M., Böhm, O., Brázdil, R., ... Wetter, O. (2020). Current European flood-rich period exceptional compared with past 500 years. *Nature*, *583*(7817), 560–566. doi: 10.1038/s41586-020-2478-3

Brunsell, N. A. (2010). A multiscale information theory approach to assess spatial-temporal variability of daily precipitation. *Journal of Hydrology*, *385*(1-4), 165–172. doi: 10.1016/j.jhydrol.2010.02.016

Buttle, J. M., Allen, D. M., Caissie, D., Davison, B., Hayashi, M., Peters, D. L., ... Whitfield, P. H. (2016). Flood processes in Canada: Regional and special aspects. *Canadian Water Resources Journal / Revue canadienne des ressources hydriques*, *41*(1-2), 7–30. doi: 10.1080/07011784.2015.1131629

Camporeale, C., Perona, P., Porporato, A., & Ridolfi, L. (2005). On the long-term behavior of meandering rivers. *Water Resources Research*, *41*(12). doi: 10.1029/2005WR004109

Chakrapani, G. J. (2005). Factors controlling variations in river sediment loads. *Current science*, 569–575.

Chen, C. F., Son, N. T., & Chang, L. Y. (2012). Monitoring of rice cropping intensity in the upper Mekong Delta, Vietnam using time-series MODIS data. *Advances in Space Research*, *49*(2), 292–301. doi: 10.1016/j.asr.2011.09.011

Constantine, J. A., & Dunne, T. (2008). Meander cutoff and the controls on the production of oxbow lakes. *Geology*, *36*(1), 23–26. doi: 10.1130/G24130A.1

Davidson, N. C., Fluet-Chouinard, E., & Finlayson, C. M. (2018). Global extent and distribution of wetlands: Trends and issues. *Marine and Freshwater Research*, *69*(4), 620–627. doi: 10.1071/MF17019

Dong, J., Xiao, X., Kou, W., Qin, Y., Zhang, G., Li, L., ... Moore, B. (2015). Tracking the dynamics of paddy rice planting area in 1986-2010 through time series Landsat images and phenology-based algorithms. *Remote Sensing of Environment*, *160*, 99–113. doi: 10.1016/j.rse.2015.01.004

Elith, J., Leathwick, J. R., & Hastie, T. (2008). *A working guide to boosted regression trees* (Vol. 77) (No. 4). John Wiley & Sons, Ltd. doi: 10.1111/j.1365-2656.2008.01390.x

Ellis, E., & Klein Goldewijk, K. (2019). *Anthromes 12k full dataset* [dataset]. Retrieved from `https://dataverse.harvard.edu/dataset.xhtml?persistentId=doi:10.7910/DVN/G0QDNQ` doi: 10.7910/DVN/G0QDNQ

Finotello, A., D'Alpaos, A., Bogoni, M., Ghinassi, M., & Lanzoni, S. (2020). Remotely-sensed planform morphologies reveal fluvial and tidal nature of meandering channels. *Scientific Reports 2020 10:1*, *10*(1), 1–13. doi: 10.1038/s41598-019-56992-w

Frasson, R. P. d. M., Pavelsky, T. M., Fonstad, M. A., Durand, M. T., Allen, G. H., Schumann, G., ... Yang, X. (2019). *Global database of river width, slope, catchment area, meander wavelength, sinuosity, and discharge* [dataset]. Zenodo. Retrieved from `https://doi.org/10.5281/zenodo.2582500` doi: 10.5281/zenodo.2582500

Gardner, J. R., Yang, X., Topp, S. N., Ross, M. R., Altenau, E. H., & Pavelsky, T. M. (2021). The Color of Rivers. *Geophysical Research Letters*, *48*(1), e2020GL088946. doi: 10.1029/2020GL088946

Gorelick, N., Hancher, M., Dixon, M., Ilyushchenko, S., Thau, D., & Moore, R. (2017). Google Earth Engine: Planetary-scale geospatial analysis for everyone. *Remote Sensing of Environment*, *202*, 18–27. doi: 10.1016/j.rse.2017.06.031

Griffin-Nolan, R. J., Slette, I. J., & Knapp, A. K. (2021). Deconstructing precipitation variability: Rainfall event size and timing uniquely alter ecosystem dynamics. *Journal of Ecology*, *109*(9), 3356–3369. doi: 10.1111/1365-2745.13724

Houspanossian, J., Kuppel, S., Nosetto, M. D., Di Bella, C. M., Oricchio, P., Barrucand, M., ... Jobbágy, E. G. (2018). Long-lasting floods buffer the thermal regime of the Pampas. *Theoretical and Applied Climatology*, *131*(1-2), 111–120. doi: 10.1007/s00704-016-1959-7

Junk, W., Bayley, P., & Sparks, R. (1989). The flood pulse concept in river-floodplain systems. *Canadian Special Publication of Fisheries and Aquatic Sciences*, *106*(Canadian Special Publication of Fisheries and Aquatic Sciences), 110–127.

Kireeva, M. B., Rets, E. P., Frolova, N. L., Samsonov, T. E., Povalishnikova, E. S., Entin, A. L., ... Ivanov, A. M. (2020). Occasional floods on the rivers of russian plain in the 20th –21st centuries. *Geography, Environment, Sustainability*, *13*(2), 84–95. doi: 10.24057/2071-9388-2020-29

Kundzewicz, Z. W. (2008). Climate change impacts on the hydrological cycle. *Ecohydrology & Hydrobiology*, *8*(2-4), 195–203. doi: 10.2478/v10104-009-0015-y

Kuppel, S., Houspanossian, J., Nosetto, M. D., & Jobbágy, E. G. (2015). What does it take to flood the Pampas?: Lessons from a decade of strong hydrological fluctuations. *Water Resources Research*, *51*(4), 2937–2950. doi: 10.1002/2015WR016966

Langhorst, T., & Pavelsky, T. (2023). Global Observations of Riverbank Erosion and Accretion From Landsat Imagery. *Journal of Geophysical Research: Earth Surface*, *128*(2), e2022JF006774. doi: 10.1029/2022JF006774

Lehner, B., & Döll, P. (2004). Development and validation of a global database of lakes, reservoirs and wetlands. *Journal of Hydrology*, *296*(1-4), 1–22. doi: 10.1016/j.jhydrol.2004.03.028

Lehner, B., & Döll, P. (2004). *Global lakes and wetlands database: Lakes and wetlands grid (level 3)* [dataset]. World Wildlife Fund. Retrieved from `https://www.worldwildlife.org/publications/global-lakes-and-wetlands-database-lakes-and-wetlands-grid-level-3`

Lin, P., Pan, M., Allen, G. H., de Frasson, R. P., Zeng, Z., Yamazaki, D., & Wood, E. F. (2020). Global Estimates of Reach-Level Bankfull River Width Leveraging Big Data Geospatial Analysis. *Geophysical Research Letters*, *47*(7), e2019GL086405. doi: 10.1029/2019GL086405

Liu, G. (2022). Understanding cotton cultivation dynamics in Aksu Oases (NW China) by reconstructing change trajectories using multi-temporal Landsat and Sentinel-2 data. *Geocarto International*, *37*(15), 4406–4424. doi: 10.1080/10106049.2021.1886337

Loarie, S. R., Lobell, D. B., Asner, G. P., & Field, C. B. (2011). Land-Cover and Surface Water Change Drive Large Albedo Increases in South America*. *Earth Interactions*, *15*(7), 1–16. doi: 10.1175/2010EI342.1

McGuire, K. J., McDonnell, J. J., Weiler, M., Kendall, C., McGlynn, B. L., Welker, J. M., & Seibert, J. (2005). The role of topography on catchment-scale water residence time. *Water Resources Research*, *41*(5), 1–14. doi: 10.1029/2004WR003657

Najibi, N., & Devineni, N. (2018). Recent trends in the frequency and duration of global floods. *Earth System Dynamics*, *9*(2), 757–783. doi: 10.5194/esd-9-757-2018

Olthof, I., & Rainville, T. (2022). Dynamic surface water maps of Canada from 1984 to 2019 Landsat satellite imagery. *Remote Sensing of Environment*, *279*, 113121. doi: 10.1016/J.RSE.2022.113121

Opperman, J. J., Luster, R., McKenney, B. A., Roberts, M., & Meadows, A. W. (2010). Ecologically functional floodplains: Connectivity, flow regime, and scale. *Journal of the American Water Resources Association*, *46*(2), 211–226. doi: 10.1111/j.1752-1688.2010.00426.x

Papa, F., Güntner, A., Frappart, F., Prigent, C., & Rossow, W. B. (2008). Variations of surface water extent and water storage in large river basins: A comparison of different global data sources. *Geophysical Research Letters*, *35*(11), L11401. doi: 10.1029/2008GL033857

Papa, F., Prigent, C., Aires, F., Jimenez, C., Rossow, W. B., & Matthews, E. (2010). Interannual variability of surface water extent at the global scale, 1993–2004. *Journal of Geophysical Research*, *115*(D12), D12111. doi: 10.1029/2009JD012674

Pekel, J.-F., Cottam, A., Gorelick, N., & Belward, A. S. (2016a). High-resolution mapping of global surface water and its long-term changes. *Nature*, *540*(7633), 418–422. doi: 10.1038/nature20584

Pekel, J.-F., Cottam, A., Gorelick, N., & Belward, A. S. (2016b). *High-resolution mapping of global surface water and its long-term changes* [dataset]. Nature Publishing Group. Retrieved from `https://developers.google.com/earth-engine/datasets/catalog/JRC_GSW1_4_MonthlyHistory` doi: 10.1038/nature20584

Pi, X., Luo, Q., Feng, L., Xu, Y., Tang, J., Liang, X., ... Bryan, B. A. (2022). Mapping global lake dynamics reveals the emerging roles of small lakes. *Nature Communications*, *13*(1), 1–12. doi: 10.1038/s41467-022-33239-3

Pickens, A. H., Hansen, M. C., Hancher, M., Stehman, S. V., Tyukavina, A., Potapov, P., ... Sherani, Z. (2020). Mapping and sampling to characterize global inland water dynamics from 1999 to 2018 with full Landsat time-series. *Remote Sensing of Environment*, *243*(December 2019), 111792. doi: 10.1016/j.rse.2020.111792

Poole, G. C. (2010). Stream hydrogeomorphology as a physical science basis for advances in stream ecology. *Journal of the North American Benthological Society*, *29*(1), 12–25. doi: 10.1899/08-070.1

R Core Team. (2021). R: A language and environment for statistical computing [Computer software manual]. Vienna, Austria. Retrieved from `https://www.R-project.org/`

Radinger, J., Alcaraz-Hernández, J. D., & García-Berthou, E. (2018). Environmental and spatial correlates of hydrologic alteration in a large Mediterranean river catchment. *Science of The Total Environment*, *639*, 1138–1147. doi: 10.1016/J.SCITOTENV.2018.05.227

Richardson, J., Sangree, J., & Sneider, R. (1987). Meandering Stream Reservoirs. *Journal of Petroleum Technology*, *39*(12), 1501–1502. doi: 10.2118/15781-PA

Riley, S., DeGloria, S., & Elliot, R. (1999). A terrain ruggedness that quantifies topographic heterogeneity. *Intermountain Journal of Science*, *5*(1-4), 23–27.

Rudorff, C. M., Melack, J. M., & Bates, P. D. (2014). Flooding dynamics on the lower Amazon floodplain: 1. Hydraulic controls on water elevation, inundation extent, and river-floodplain discharge. *Water Resources Research*, *50*(1), 619–634. doi: 10.1002/2013WR014091

Sakamoto, T., Van Nguyen, N., Kotera, A., Ohno, H., Ishitsuka, N., & Yokozawa, M. (2007). Detecting temporal changes in the extent of annual flooding within the Cambodia and the Vietnamese Mekong Delta from MODIS time-series imagery. *Remote Sensing of Environment*, *109*(3), 295–313. doi: 10.1016/j.rse.2007.01.011

Saunois, M., Stavert, A. R., Poulter, B., Bousquet, P., Canadell, J. G., Jackson, R. B., ... Zhuang, Q. (2020). The Global Methane Budget 2000–2017. *Earth System Science Data*, *12*(3), 1561–1623. doi: 10.5194/essd-12-1561-2020

Siebert, S., Kummu, M., Porkka, M., Döll, P., Ramankutty, N., & Scanlon, B. R. (2015). A global data set of the extent of irrigated land from 1900 to 2005. *Hydrology and Earth System Sciences*, *19*(3), 1521–1545. doi: 10.5194/hess-19-1521-2015

Sivapalan, M., Thompson, S. E., Harman, C. J., Basu, N. B., & Kumar, P. (2011). Water cycle dynamics in a changing environment: Improving predictability through synthesis. *Water Resources Research*, *47*(10). doi: 10.1029/2011WR011377

Tena, A., Piégay, H., Seignemartin, G., Barra, A., Berger, J. F., Mourier, B., & Winiarski, T. (2020). Cumulative effects of channel correction and regulation on floodplain terrestrialisation patterns and connectivity. *Geomorphology*, *354*. doi: 10.1016/j.geomorph.2020.107034

Tockner, K., Malard, F., & Ward, J. V. (2000). An extension of the flood pulse concept. *Hydrological Processes*, *14*(16-17), 2861–2883. doi: 10.1002/1099-1085(200011/12)14:16/17⟨2861::AID-HYP124⟩3.0.CO;2-F

Tockner, K., & Stanford, J. A. (2002). Riverine flood plains: Present state and future trends. *Environmental Conservation*, *29*(3), 308–330. doi: 10.1017/S037689290200022X

Tooth, S. (2000). Process, form and change in dryland rivers: A review of recent research. *Earth Science Reviews*, *51*(1-4), 67–107. doi: 10.1016/S0012-8252(00)00014-3

Torre Zaffaroni, P., Baldi, G., Texeira, M., Di Bella, C. M., & Jobbagy, E. G. (2023). The timing of global floods and its association with climate and topography. *ESS Open Archive*. doi: 10.1002/essoar.10511955.2

Tran, D. D., van Halsema, G., Hellegers, P. J., Ludwig, F., & Wyatt, A. (2018). Questioning triple rice intensification on the Vietnamese mekong delta floodplains: An environmental and economic analysis of current land-use trends and alternatives. *Journal of Environmental Management*, *217*, 429–441. doi: 10.1016/j.jenvman.2018.03.116

Twine, T. E., Kucharik, C. J., & Foley, J. A. (2004). Effects of Land Cover Change on the Energy and Water Balance of the Mississippi River Basin. *Journal of Hydrometeorology*, *5*(4), 640–655. doi: 10.1175/1525-7541(2004)005⟨0640:EOLCCO⟩2.0.CO;2

Van Dijk, W. M., Van de Lageweg, W. I., & Kleinhans, M. G. (2013). Formation of a cohesive floodplain in a dynamic experimental meandering river. *Earth Surface Processes and Landforms*, *38*(13), 1550–1565. doi: 10.1002/ESP.3400

Vörösmarty, C. J., McIntyre, P. B., Gessner, M. O., Dudgeon, D., Prusevich, A., Green, P., ... Davies, P. M. (2010). Global threats to human water security and river biodiversity. *Nature*, *467*(7315), 555–561. doi: 10.1038/nature09440

Walcker, R., Corenblit, D., Julien, F., Martinez, J.-M., & Steiger, J. (2021). Contribution of meandering rivers to natural carbon fluxes: Evidence from the Ucayali River, Peruvian Amazonia. *Science of The Total Environment*, *776*, 146056. doi: 10.1016/j.scitotenv.2021.146056

Wantzen, K. M., Junk, W. J., & Rothhaupt, K.-O. (2008). An extension of the floodpulse concept (FPC) for lakes. In *Ecological effects of water-level fluctuations in lakes* (pp. 151–170). Dordrecht: Springer Netherlands. doi: 10.1007/978-1-4020-9192-6_15

Ward, J. V., & Stanford, J. A. (1995). Ecological connectivity in alluvial river ecosystems and its disruption by flow regulation. *Regulated Rivers: Research & Management*, *11*(1), 105–119. doi: 10.1002/rrr.3450110109

Watts, J. D., Kimball, J. S., Bartsch, A., & McDonald, K. C. (2014). Surface water inundation in the boreal-Arctic: Potential impacts on regional methane emissions. *Environmental Research Letters*, *9*(7), 075001. doi: 10.1088/1748-9326/9/7/075001

Wren, D. G., Davidson, G. R., Walker, W. G., & Galicki, S. J. (2008). The evolution of an oxbow lake in the Mississippi alluvial floodplain. *Journal of Soil and Water Conservation*, *63*(3), 129–135. doi: 10.2489/jswc.63.3.129

Wu, J., Zhang, Q., Li, Y., Xu, C. Y., & Ye, X. (2023). Spatial-temporal variations of stage-area hysteretic relationships in large heterogeneous lake–floodplain systems. *Journal of Hydrology*, *620*, 129507. doi: 10.1016/j.jhydrol.2023.129507

Zeng, Z.-H., Lu, Z.-Y., Jiang, Y., Zhang, K., Yang, Y.-D., & Zhao, P.-Y. (2016). Legume-cereal crop rotation systems in china. *Crop Rotations: Farming Practices, Monitoring and Environmental Benefits. Ottawa, ON, Canada: Nova Science Publishers*, 51–70.

Figure 1.

a)	b) case 1	c) case 2	d) case 3	e) case 4
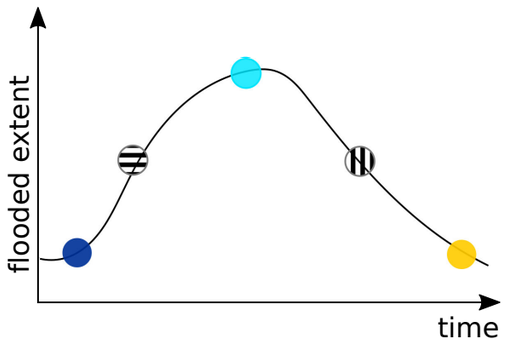	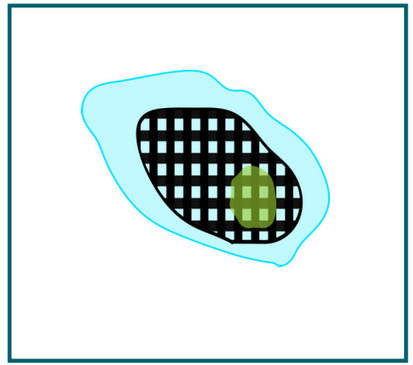	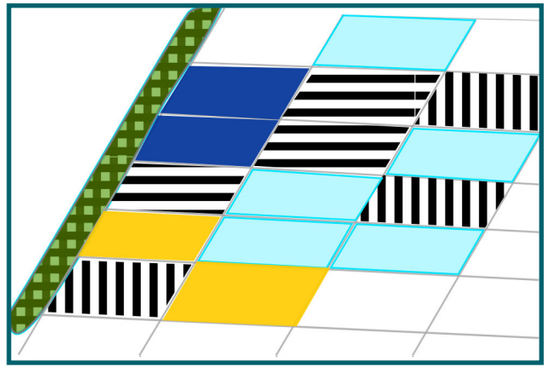	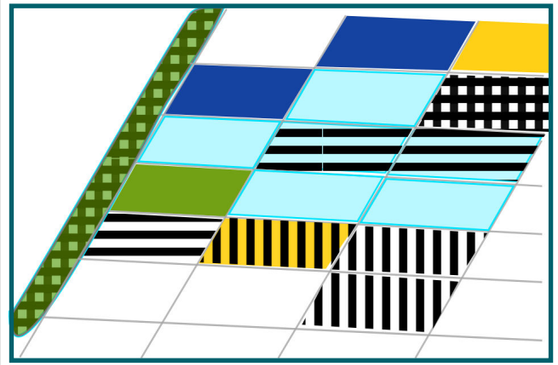	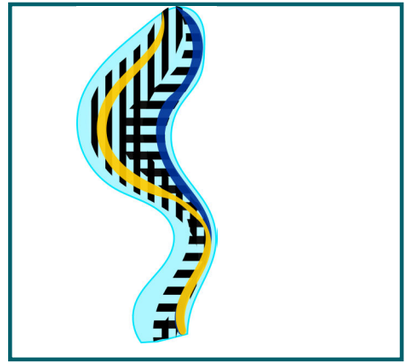
is the variability spatially coherent?	Y	N	N	N
is the *extreme displacement* index (d*ext*) able to capture the displacement?		Y	Y, but underestimates	N
is the *total displacement* index (d*tot*) able to capture the displacement?		Y	Y	Y

Figure 2.

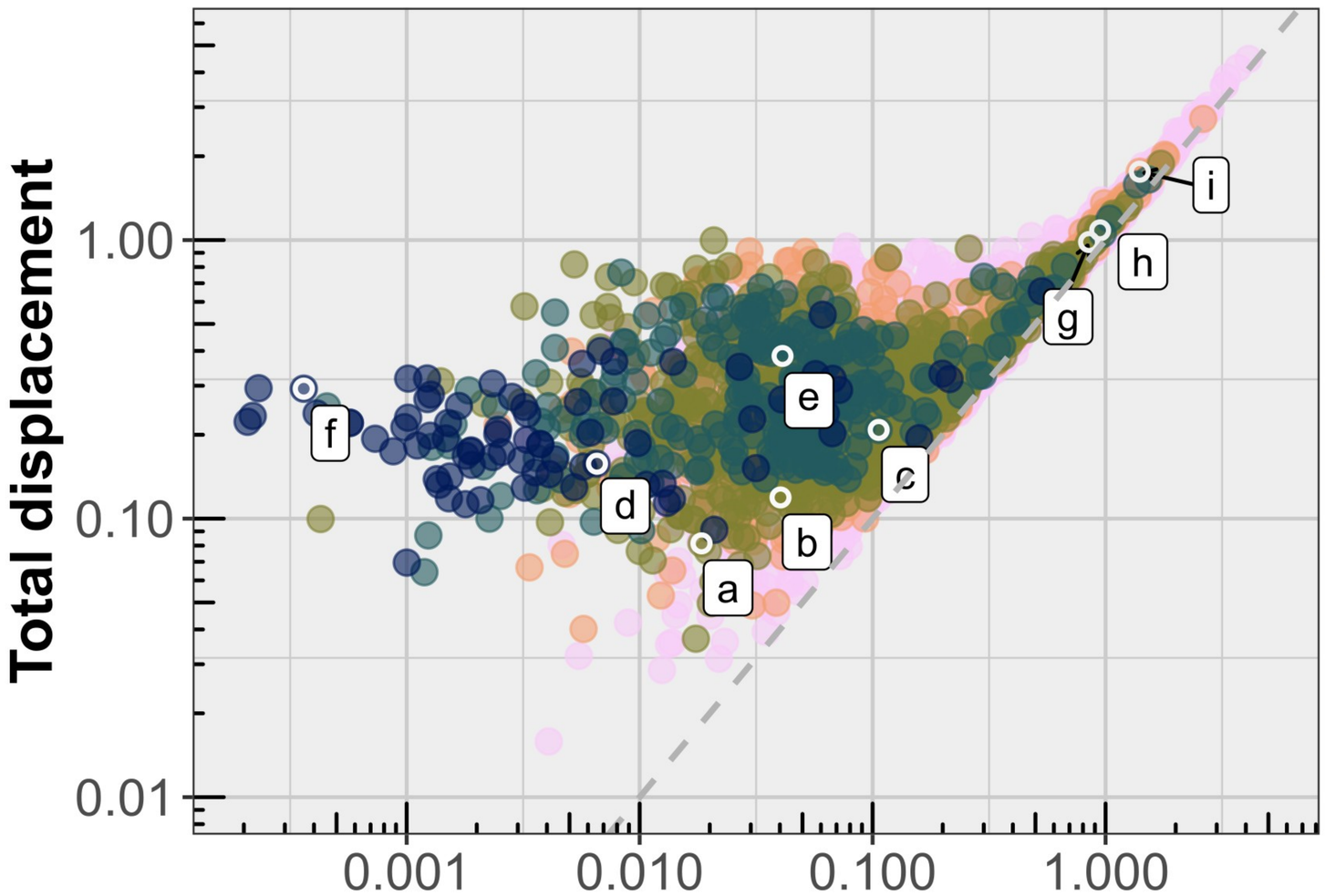

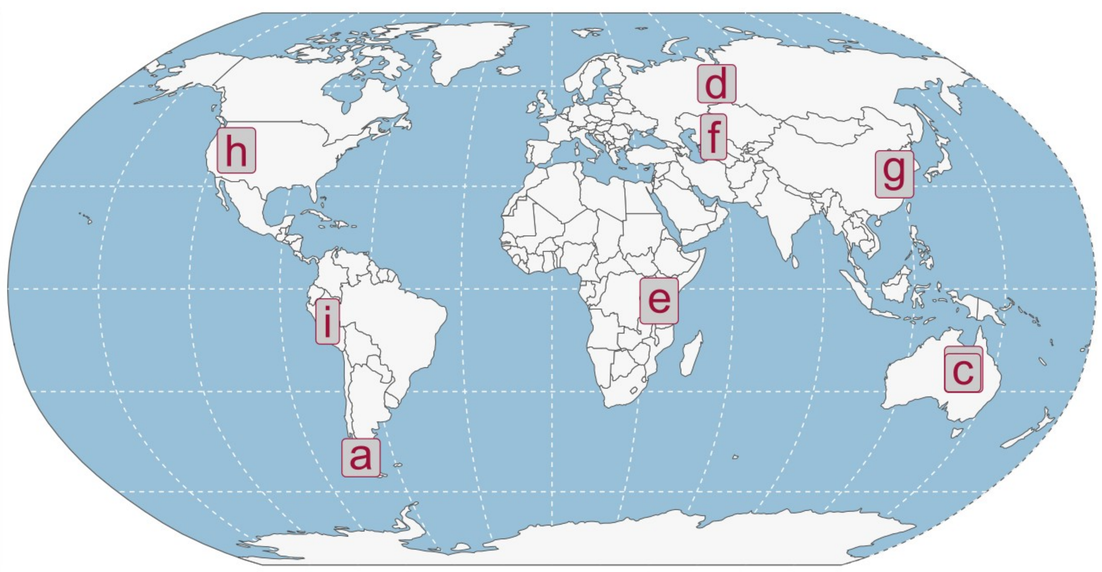

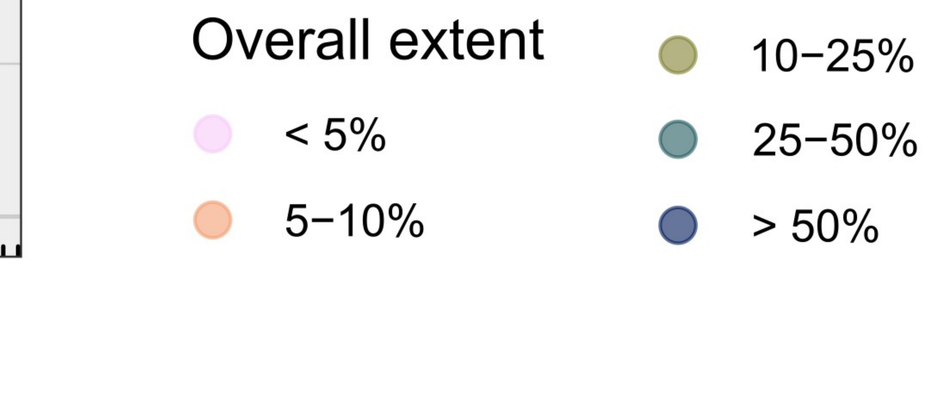

Extreme displacement

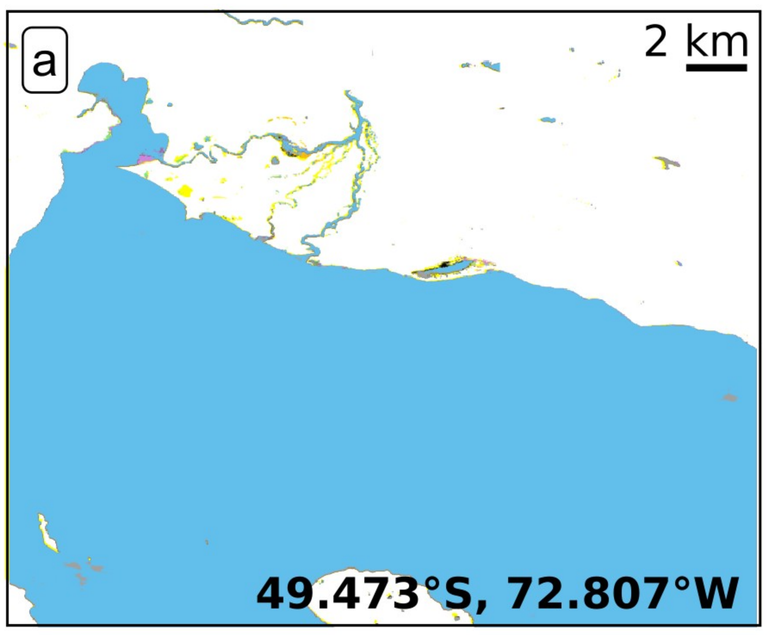

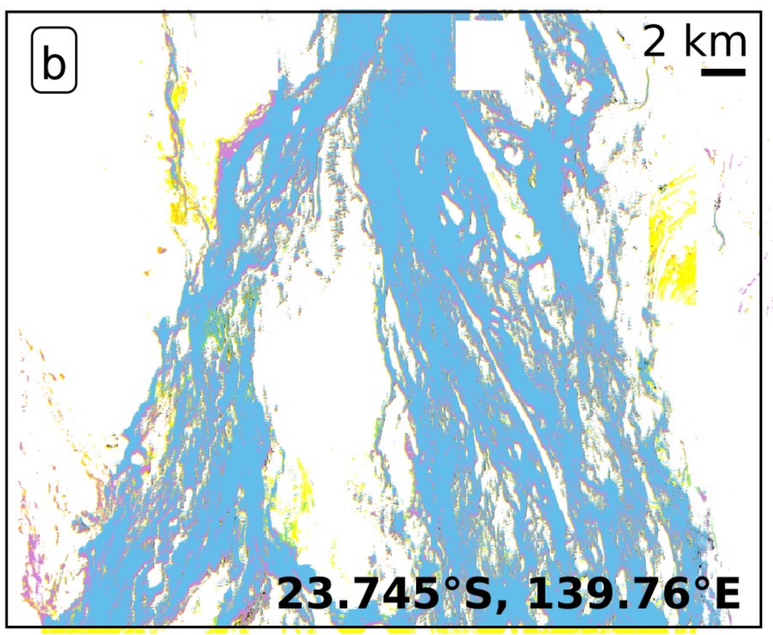

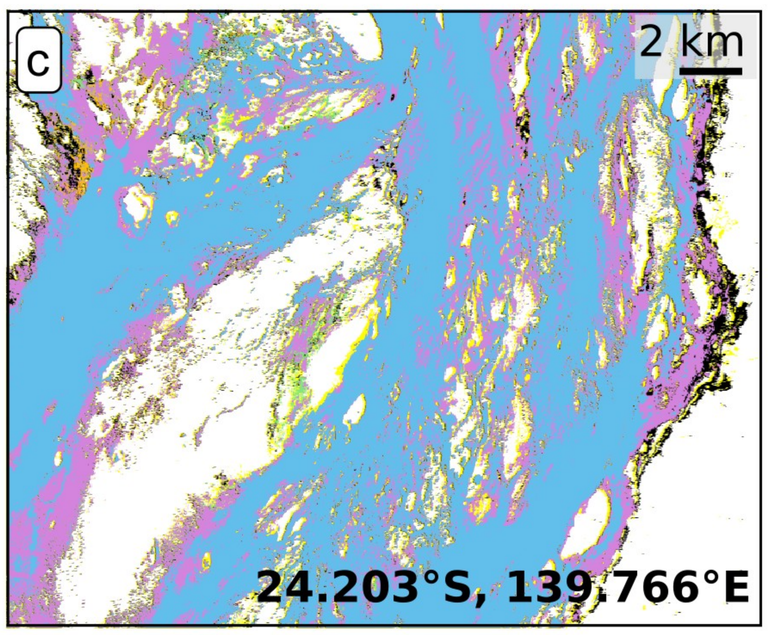

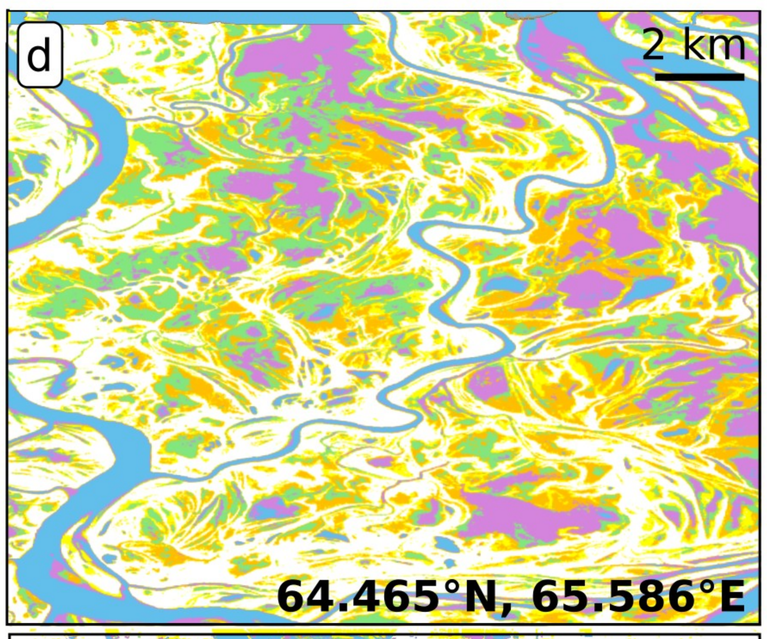

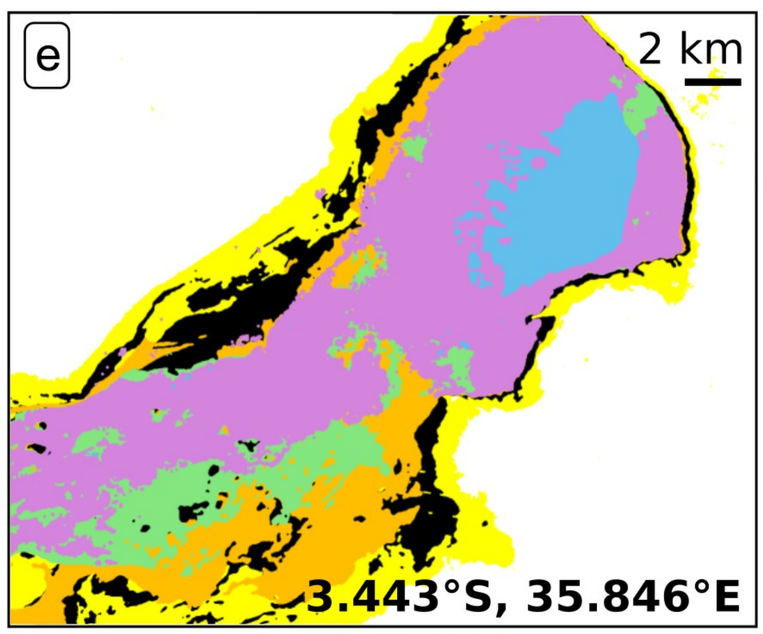

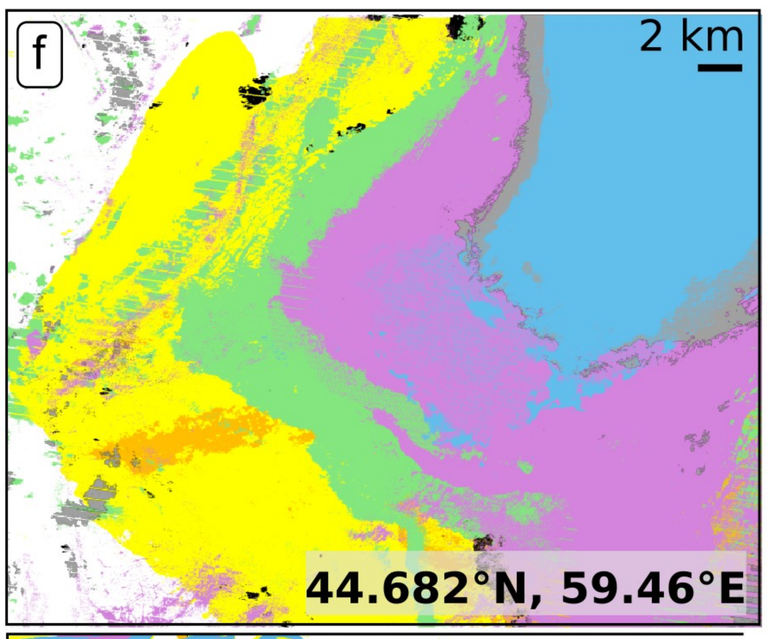

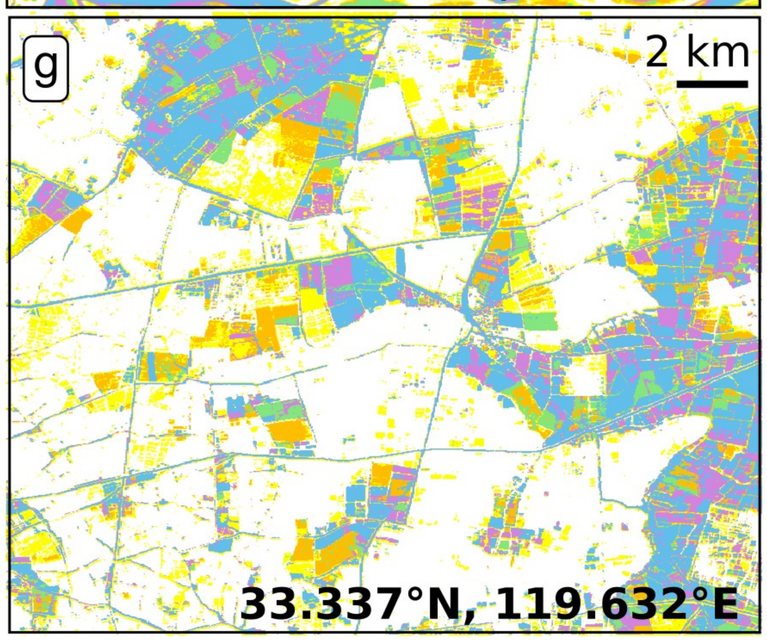

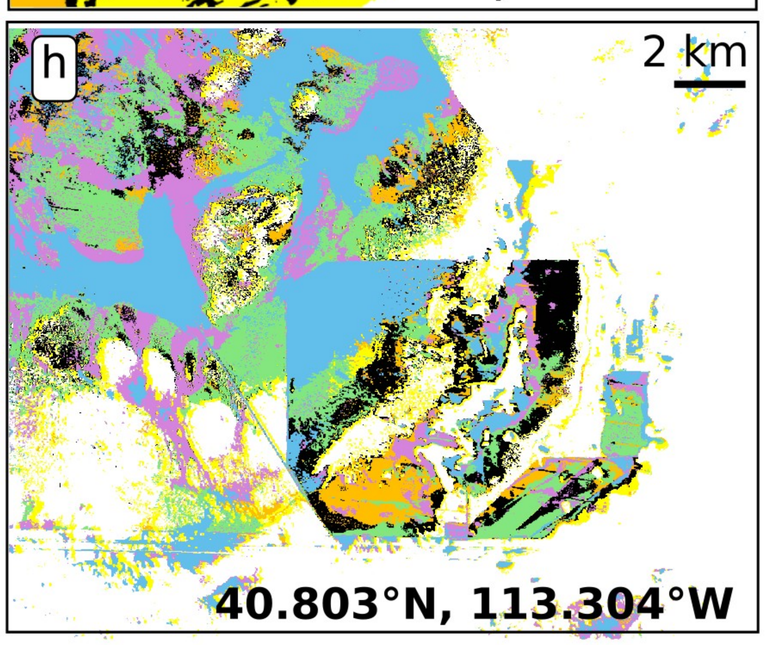

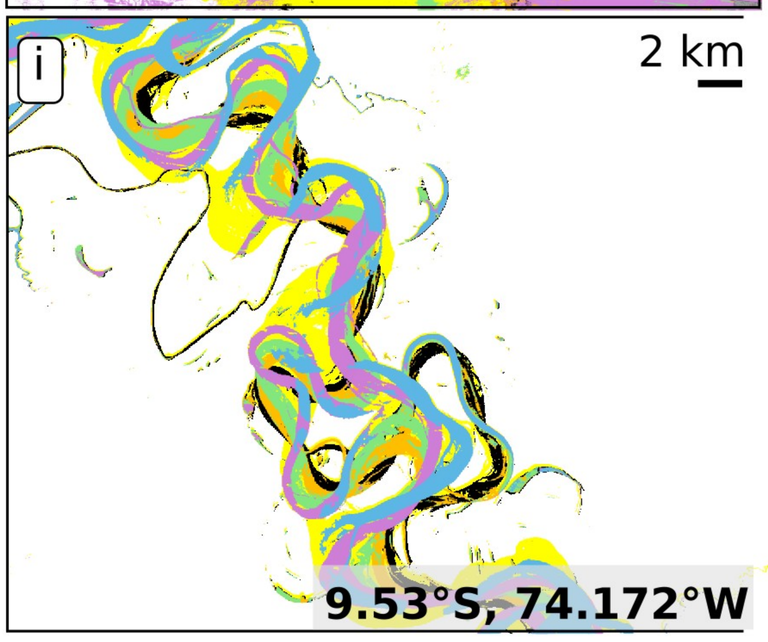

Figure 3.

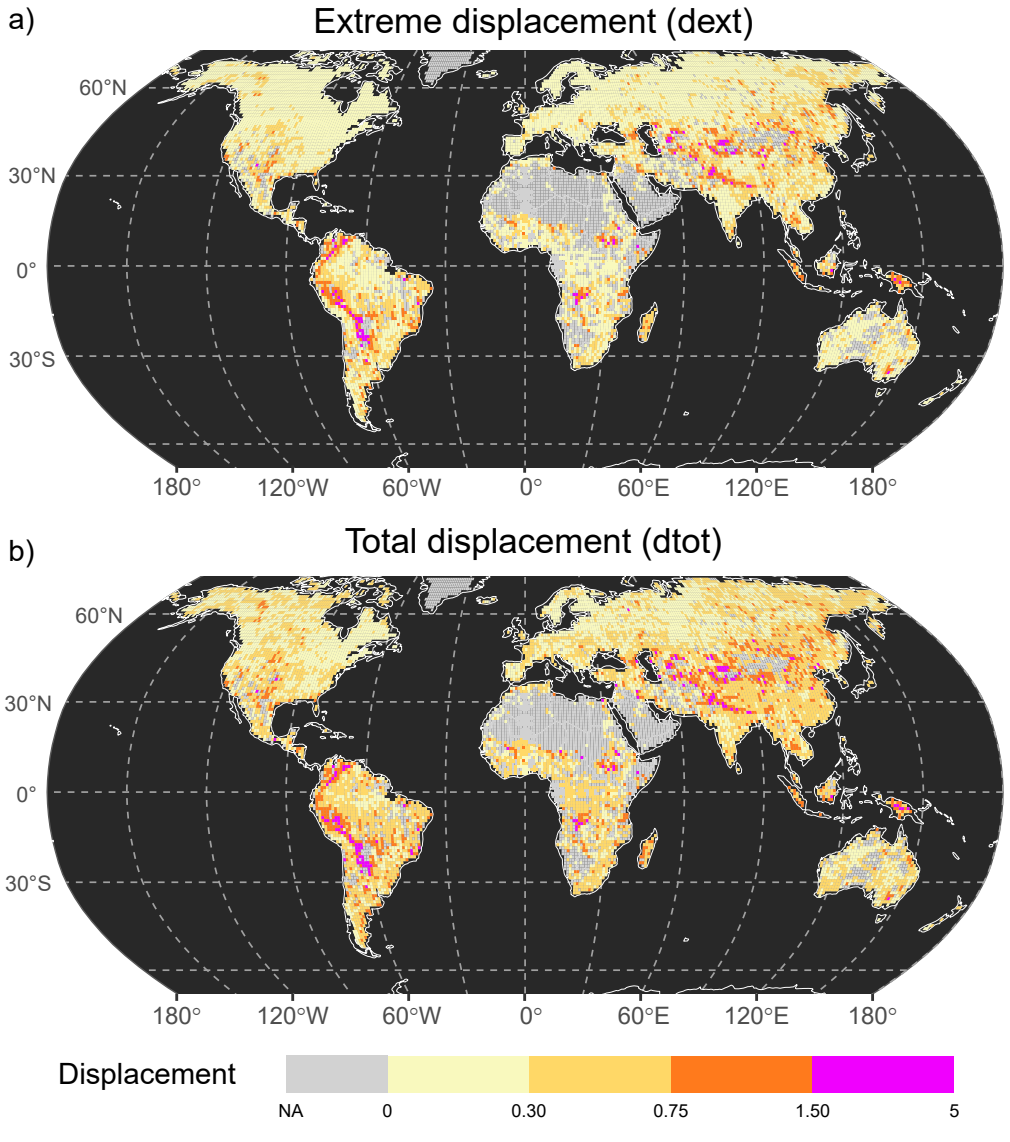
a)
Extreme displacement (dext)
60°N
30°N
0°
30°S
180°
120°W
60°W
0°
60°E
120°E
180°
b)
Total displacement (dtot)
60°N
30°N
0°
30°S
180°
120°W
60°W
0°
60°E
120°E
180°
Displacement
NA
0
0.30
0.75
1.50
5